Molecular Dynamics Study of Ethanolamine as a Pure Liquid and in Aqueous Solution

ARTICLE *in* THE JOURNAL OF PHYSICAL CHEMISTRY B · MAY 2007

Impact Factor: 3.3 · DOI: 10.1021/jp068227p · Source: PubMed

4 AUTHORS, INCLUDING:

Tatyana Kuznetsova
University of Bergen
59 PUBLICATIONS **688** CITATIONS
SEE PROFILE

Bjørn Kvamme
University of Bergen
364 PUBLICATIONS **1,650** CITATIONS
SEE PROFILE

Kenneth M Merz
Michigan State University
273 PUBLICATIONS **23,757** CITATIONS
SEE PROFILE

Molecular Dynamics Study of Ethanolamine as a Pure Liquid and in Aqueous Solution

Eirik F. da Silva,*,†,‡ Tatyana Kuznetsova,§ Bjørn Kvamme,§ and Kenneth M. Merz Jr.||

Department of Chemical Engineering, Norwegian University of Science and Technology, N-7491 Trondheim, Norway, SINTEF Materials and Chemistry, R. Birkelands vei 2B, NO-7465 Trondheim, Norway, Department of Physics, University of Bergen, N-5007 Bergen, Norway, and Quantum Theory Project, University of Florida, Gainesville, Florida 32611

Received: November 30, 2006; In Final Form: February 9, 2007

Molecular dynamics simulations have been carried out for ethanolamine as a pure liquid and in aqueous solution at 298 and 333 K. The ethanolamine force field has been parametrized to reproduce intramolecular energies from quantum mechanical calculations and experimentally determined properties of the liquid. The results are presented for conformer distributions, density, enthalpy of vaporization, self-diffusion constant, dielectric constant, and radial distribution functions. The results strongly suggest that the main (O−C−C−N) dihedral tends to stay in its gauche conformers in solution and that the ethanolamine molecules populate conformers with a significant degree of intramolecular hydrogen bonding. This result is also supported by results from a continuum solvation model. Simulation of a 10 mol % aqueous ethanolamine system suggests that ethanolamine is preferentially solvated to by water molecules. The results suggest that ethanolamine dimer formation in aqueous solution is very limited. Simulations were also carried out for CO_2 in an aqueous ethanolamine system. The results suggest that CO_2 has a comparable level of attraction to ethanolamine and water. The degree of interaction between CO_2 and the amine and alcohol functionalities in ethanolamine also appear to be of comparable strength.

Introduction

Mixtures of alkanolamines and water are commonly used to absorb CO_2 from natural gas and exhaust gases.[1] Chemical absorption is currently one of the most viable among the available technologies to capture CO_2.[2] While alkanolamine-based CO_2 capture has received considerable experimental attention, little work has been done on the understanding of these systems at the molecular level. Ethanolamine (shown in Figure 1) is the simplest of the alkanolamine molecules, and some simulation work has been done in recent years to ascertain its liquid structure and properties, as well as its behavior in aqueous solution.[3−8]

Ethanolamine and other alkanolamines are an interesting class of molecules. Together with 1-2 ethanediol, ethanolamine represents one of the simplest molecules able to form intramolecular hydrogen bonds. Both in pure liquids and in aqueous solutions intramolecular hydrogen bonding will compete with the formation of intermolecular hydrogen bonds. This potential for hydrogen bonding also raises questions about the structure of ethanolamine both as a pure liquid and in aqueous solution. The modeling of such small organic molecules is also of relevance to the modeling of more complex biomolecules.

In the parametrization of molecular force fields, ethanolamine and other alkanolamines present a significant challenge. Two main approaches for parametrization of force fields exist in the literature. For water and small organic molecules, such as methanol, a number of specially fitted force fields have been presented (Guillot[9] and Walser et al.[10] and references therein). These are typically based on reproducing certain experimental properties, such as density, radial distribution functions, and enthalpy of vaporization, and each parameter in the force field is often fine-tuned. This approach to force field fitting is not viable in the case of larger organic molecules with many atomic sites and many degrees of freedom. For such molecules, transferable force fields such as OPLS[11] have been developed. Ethanolamine is a relatively small molecule, but the number of parameters in a force field will tend to be much higher than that for water, and the molecule has not been as rigorously studied experimentally as water or simple mono-alcohols. However, there appears to be room for more detailed force field parametrization than that usually seen for biomolecules.

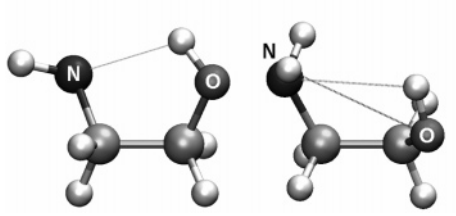

Figure 1. g′Gg′ and tGg′ conformers of ethanolamine.

The intention of the present work has been to look in greater detail at force field parametrization, conformer distribution, and other aspects of the system of particular relevance to the gas absorption process. The liquid structure is highly relevant to understanding the reaction mechanisms of CO_2 absorption. While the classical simulations utilized in the present work cannot be directly used to model the reactions in the system, it can help to elucidate reaction mechanisms. We are especially interested in understanding the barriers in the carbamate formation reaction, which can be written in the following form:[12]

$$CO_2 + R_1R_2NH\cdots B \rightleftharpoons R_1R_2NCOO^-\cdots BH^+ \qquad (1)$$

* To whom correspondence should be addressed. E-mail: Eirik.Silva@sintef.no.
† Norwegian University of Science and Technology.
‡ SINTEF Materials and Chemistry.
§ University of Bergen.
|| University of Florida.

10.1021/jp068227p CCC: $37.00
Published on Web 03/22/2007

TABLE 1: Force Fields for Ethanolamine

bond	r_0 (Å)	k_r[a]
N−H	1.018	394.1
N−C	1.470	320.6
C−C	1.535	303.1
C−O	1.426	314.1
C−H	1.093	335.9
O−H	0.974	369.6

angle	θ_0	k_θ[b]
H−N−H	109.50	35.0
H−N−C	116.78	46.0
N−C−C	110.38	66.2
C−C−O	109.43	67.7
C−C−H	110.07	46.4
C−O−H	108.16	47.1

dihedral	C_1[c]	C_2[c]	C_3[c]
H−N−C−C (MEAa)	−1.29	−0.59	0.82
O−C−C−N (MEAa)	−1.02	−0.08	1.1556
C−C−O−H (MEAa)	−0.43	0.0	−0.07
H−N−C−C (MEAo)	−1.37	−0.6	0.82
O−C−C−N (MEAo)	−1.02	−0.11	1.1556
C−C−O−H (MEAo)	−0.21	0.17	−0.07

site	R* (Å)	ϵ (kcal mol^{-1})	q (MEAa)[d]	q (MEAo)[e]
H(N)	0.600	0.0157	0.335	0.36
N	1.824	0.1700	−0.88	−0.9
C(N)	1.908	0.1094	0.2	0.06
C(O)	1.908	0.1094	0.25	0.145
O	1.721	0.2104	−0.6	-0.683
H(O)	0.0	0.0	0.36	0.418
H(C)	1.387	0.0157	0.0	0.06

[a] kcal mol^{-1} Å^{-2}. [b] kcal mol^{-1} radian^{-2}. [c] kcal mol^{-1}. [d] Charges from fitting to electrostatic potential. [e] OPLS all-atom force field charges.

In an ethanolamine−water system, both B (a base molecule) and R_1R_2NH would be ethanolamine molecules. The dotted line indicates a hydrogen bond. The mechanism may also be two-step, with CO_2 first bonding with the amine to form a zwitterion, with proton transfer to a base molecule being the second step.[12]

An industrial CO_2 absorption process with ethanolamine−water is often run at temperatures ranging from around 330 to 390 K. The process is often run with ethanolamine concentrations of 10 mol %, corresponding to around 30 wt %. In the parametrization of ethanolamine, we will focus on reproducing the properties of ethanolamine at 333 K. This choice is partly due to the relevance of temperature to the process but also because the experimental heat of vaporization of ethanolamine is available at this temperature.

Simulations are carried out for pure ethanolamine, ethanolamine in infinite dilution in water, and a 10 mol % ethanolamine system. The 10 mol % ethanolamine system is included because of its direct relevance to the absorption process.

Force Field. In developing the present force field, the goal has been to reproduce experimentally observed properties of liquid ethanolamine while utilizing a standard intramolecular potential. The intramolecular potential has been fitted to conformer energies and rotational energy barriers obtained from quantum mechanical calculations. The experimental properties being reproduced are the density and heat of vaporization. This force field development approach is similar to that adopted by Jorgensen and co-workers in the development of the OPLS force field.[11]

While simulation work on ethanolamine has been reported in the literature, it appears to us that little attention has been given to the quality of the intramolecular potential in the force fields, rather the focus has been on intermolecular interactions.

TABLE 2: Relative Conformer Energies[a]

	B3LYP[b]	MEAa	MEAo
g′Gg′	0	0	0
gGg′	1.31	1.1	1.5
gGt	1.27	1.9	e
tGt	1.37	1.3	1.7
tGg	1.57	0.8	0.6
gGg	1.64	2.4	2.8
tGg′	2.27	1.8	1.8
tTt	2.31	3.5[c]	e
tTg	2.51	2.4	1.8
gTt	1.91	2.5	2.6
gTg	2.51	2.2	1.9
g′Tg	2.53	2.9	2.7
g′Gt	3.86	7.0[d]	e
g′Gg	4.83[c]	6.4[d]	e

[a] Values in kcal mol^{-1}. [b] Sum of electronic and zero-point energies at the B3LYP/6-311++G(2d,2p) level from Vorobyov et al.[18] [c] No local minima, value obtained in restrained optimization at the B3LYP/6-311++G(2d,2p) level (N−C−C−O, 63.4; C−C−O−H, 71.7; C−C−N−H1, -161.4; and C−C−N−H2, 78.7); no zero-point energy correction. [d] No local minima in force field, values obtained by restraining dihedrals to B3LYP/6-311++G(2d,2p) values. [e] No local minima in force field.

For a flexible molecule such as ethanolamine, the nature of the intramolecular potential may have a significant effect on the liquid properties.

The present force field is in a conventional all-atom form. Bond lengths and bond angles are handled by harmonic potentials

$$U(r) = k_r(r - r_0)^2 \tag{2}$$

and

$$U(\theta) = k_\theta(\theta - \theta_0)^2 \tag{3}$$

where r and θ are the bond lengths and bond angles, respectively. The subscript 0 denotes the equilibrium value. k_θ is the spring constant. Dihedral angle energies around bonds are given by

$$U(\phi) = \sum_{\text{dihedrals}} C_n \cos(n\phi) \tag{4}$$

where ϕ is the dihedral angle and the C_n values are constants. The potential energy is given by the usual combination of Lennard-Jones and Coulomb potentials

$$U(r_{ij}) = \left[\left(\frac{A_{ij}}{r_{ij}}\right)^{12} - \left(\frac{R_{ij}}{r_{ij}}\right)^{6}\right] + \frac{q_i q_j}{r_{ij}} \tag{5}$$

where q values are the atomic charges and i and j are any atomic sites. $A_{ij} = \epsilon_{ij}(R_{ij}^*)^{12}$ and $B_{ij} = 2\epsilon_{ij}(R_{ij}^*)^6$. The Lennard-Jones and Coulomb potentials are applied to atom pairs separated by three bonds or more. The 1-4 Lennard-Jones and Coulomb interactions are left unscaled in the present force field. In the development of this force field, several common 1-4 scaling factors were tested, however, such scaling resulted in an overestimation of the strength of the intramolecular hydrogen bonds. Leaving the 1-4 interactions unscaled is the same choice taken by Kirschner and Woods[13] in developing force fields for carbohydrates. Carbohydrates are similar to ethanolamine in that they have the potential to form strong intramolecular hydrogen bonds.

The parameters for the ethanolamine force field are shown in Table 1. Parameters for the bonds, angles, and Lennard-Jones

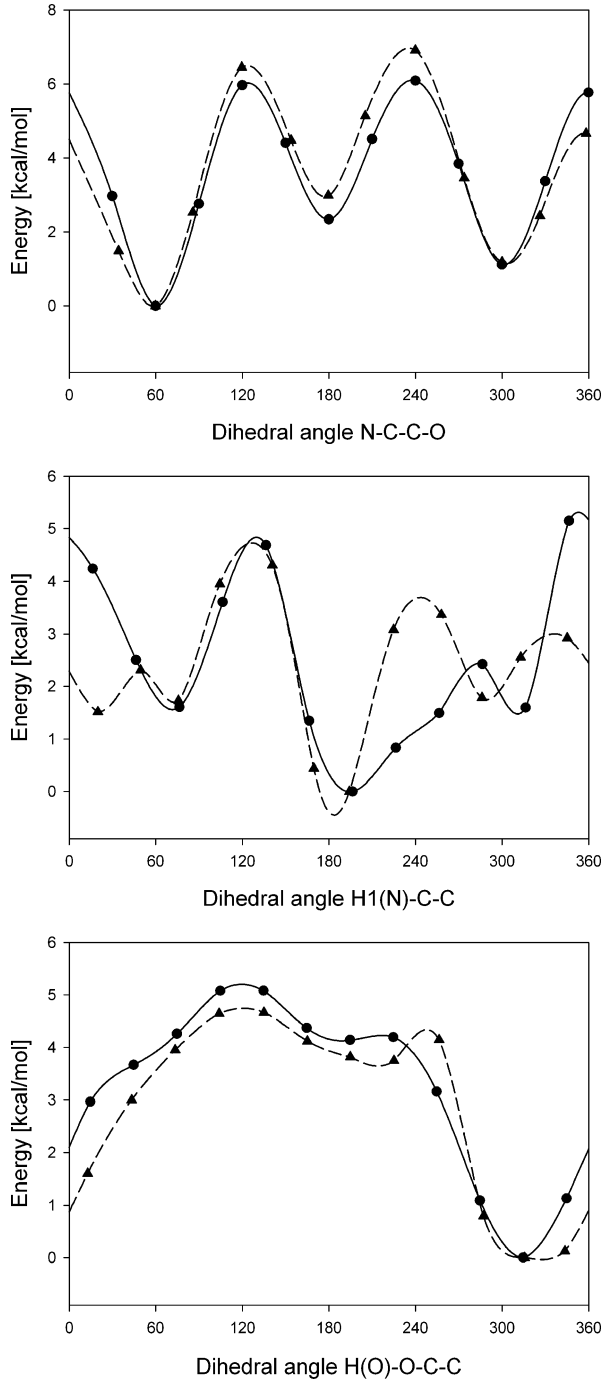

Figure 2. Rotational energy barriers for ethanolamine. Circles connected by solid lines are HF/6-311++G(2d,2p) results, and triangles connected by dashed lines are MEAa force field.

potential were drawn from the General Amber Force Field (GAFF).[14] These parameters could also have been drawn from other general force fields and/or quantum mechanical calculations. These parameters do not vary that much between force fields, and small changes are unlikely to have a large effect on the overall performance of the force field.

The charges were determined by scaling charges fitted to the electrostatic potential from quantum mechanical calculations. Charges fitted to the electrostatic potential were calculated with the Merz−Kollman scheme.[15] Calculations were carried out in Gaussian 98[16] at the B3LYP/6-311++G(d,p) level on the most stable (gas phase) conformer. All charges were then scaled by a single scaling factor to reproduce the density and enthalpy of vaporization of liquid ethanolamine at 333 K. Simulations were

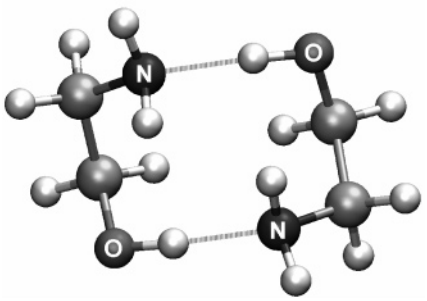

Figure 3. Cyclical dimer of ethanolamine.

carried out with a number of different scaling factors to obtain the best overall agreement for the two properties. The scaling factor adopted was 0.96, and charges were rounded off so that all H(C) had a charge of 0 and that the two H(N) atoms were given the same charge. This force field will be referred to as MEAa in the text (MEA is the common acronym for ethanolamine). It should be noted that charges fitted to the electrostatic potential do vary with the level of theory and conformer form. In the present scheme where the charges are scaled to fit experimental data, these effects are, however, of less concern.

An OPLS-like force field was also tested. Charges for this force field were drawn from the general all-atom OPLS force field;[11,17] torsions were fitted by the same scheme as that used for MEAa while other parameters were set the same as in the MEAa (details in Table 1). This force field will be referred to as MEAo.

After a set of charges were selected, the torsional terms were fitted to reproduce conformer energies and rotational energy barriers. The conformer energies are fitted to the B3LYP/6-311++G(2d,2p) level energies reported by Vorobyov et al.[18] Rotational barriers were calculated at the Hartree−Fock (HF)/6-311++G(2d,2p) level (calculations performed in Gaussian 98[16]). Both HF and force field rotational barrier calculations were carried out with partial geometry optimizations on a molecule where one dihedral was fixed. In all cases, the most stable gas-phase conformer was selected as input geometry.

In the fitting, the C_3 torsional constants (in eq 4) were mainly set to reproduce the rotation barriers, while the other terms were fitted to conformer energies. Priority was given to reproducing the balance between N−C−C−O gauche and trans conformers. Conformer energies are shown in Table 2, and rotational energies are shown in Figure 2. The conformer notation has been adopted from work by Vorobyov et al.[18] A conformer is represented as *xYz*. Where *x* designates the C−C−N− *lp*N dihedral angle, *Y* is the O−C−C−N dihedral angle, and *z* the C−C−O−H dihedral angle. *lp*N denotes the lone pair on the nitrogen atom. G or g indicates gauche(+), G′ or g′ indicates gauche(-), and T or t indicates trans.

In quantum mechanical calculations, cyclic dimer forms of ethanolamine have been identified.[18] The most stable cyclic dimer involves two ethanolamine molecules bonded by H(O)−N hydrogen bonds. Figure 3 shows the dimer structure obtained from calculations with the MEAa force field in vacuum. The dimer formation energy was −8.6 kcal mol^{-1}. The zero-point energy corrected B3LYP/6-311++(2d,2p) formation energy reported by Vorobyov et al.[18] for the same dimer was −8.8 kcal mol^{-1}. This result suggests that the present force field has a realistic dimer formation energy.

For water, the TIP3P solvent model was chosen.[19] The water model was chosen to be compatible with the ethanolamine force field. TIP3P is a widely used model that is often used together

TABLE 3: Densities, Heats of Vaporization, and Dielectric Constants for MEA (ethanolamine) and Water

	MEAa and TIP3P	MEAo	experimental
ñ (333 K)[a] for MEA	1.021	1.076	0.984[d]
ΔH_{vap} (333 K)[b] for MEA	13.24	17.75	13.79[e]
ϵ_o for MEA	37.5 ± 10		26[f]
ñ (333 K) for water	0.952		0.983[d]
ñ (333 K) for 10% MEA[f]	0.97		0.992[d]

[a] Density in g/cm^3. [b] Enthalpy of vaporization in kcal mol^{-1}. [c] 10 mol % ethanolamine in water at 333 K. [d] Data from Cheng et al.[24] [e] Data from da Silva[5] and references therein. [f] Data from Austgen et al.[25]

TABLE 4: Conformer Populations

	MEAa	MEAo	inf. dil.[a]	SM 5.42R[b]
	333 K	333 K	333 K	298 K
g′Gg′	0.07	0.02	0.04	0.11
gGg′	0.07	0.04	0.06	0.06
gGt	0.02	0.01	0.03	0.20
tGt	0.12	0.06	0.14	0.14
tGg	0.25	0.19	0.25	0.03
gGg	0.03	0.01	0.05	0.12
tGg′	0.28	0.33	0.26	0.05
tTt	0.02	0.04	0.02	0.07
tTg	0.06	0.21	0.07	0.01
gTt	0.01	0.02	0.02	0.03
gTg	0.02	0.04	0.02	0.02
g′Tg	0.02	0.03	0.02	0.04
g′Gt	0.00	0.00	0.01	0.10
g′Gg	0.02	0.00	0.02	0.00

[a] MEAa in infinite dilution aqueous solution. [b] Gas-phase energy from Vorobyov et al.[18] and solvation energy calculated at the SM 5.42R/HF/6-31G(d)// HF/6-31G(d) level of theory.[27] Calculation carried out in Gamesol.[28]

with the AMBER[12] force fields and the OPLS force field that the present ethanolamine representation draws on.

A modified version of the EMP2 model[20] has been utilized to represent CO_2. The modification consists of fitting the angle spring constant to energies from quantum mechanical calculations. B3LYP/6-311++G(d,p) calculations were carried out for unconstrained CO_2 and CO_2 with constrained bond angle. Constrained calculations were carried out with bond angles varying between 180° and 150°. The spring constant was set to reproduce the variations in energy with bond angles from these calculations. The model details together with the fitted data are given in the Supporting Information. It should be noted that while the original EMP2 spring constant was fitted to experimental data, the constants are quite similar. The present spring constant is 56.47 cal degree^{-2} mol^{-1}, while the EMP2 spring constant is 45 cal degree^{-2} mol^{-1}.

Force field parameters are sensitive to the implementation details of simulation codes. The codes do, for example, vary in the handling of bonds, cutoffs, choice of thermostat, and pressure control algorithm. All of which may affect properties such as densities and enthalpies.

Simulations Details. Simulations were carried out in an NPT ensemble in the molecular dynamics code AMBER 9.[21] The particle-mesh Ewald procedure was used to handle long-range electrostatic interactions. Temperature was controlled by Langevin dynamics, while pressure was controlled by weak coupling to an external bath. Simulations were carried out at a pressure of 1 bar and temperatures of 333 and 298 K. The nonbonded cutoff was set to 10 Å for all simulations. Bonds length involving hydrogen atoms were maintained by use of a SHAKE algorithm.

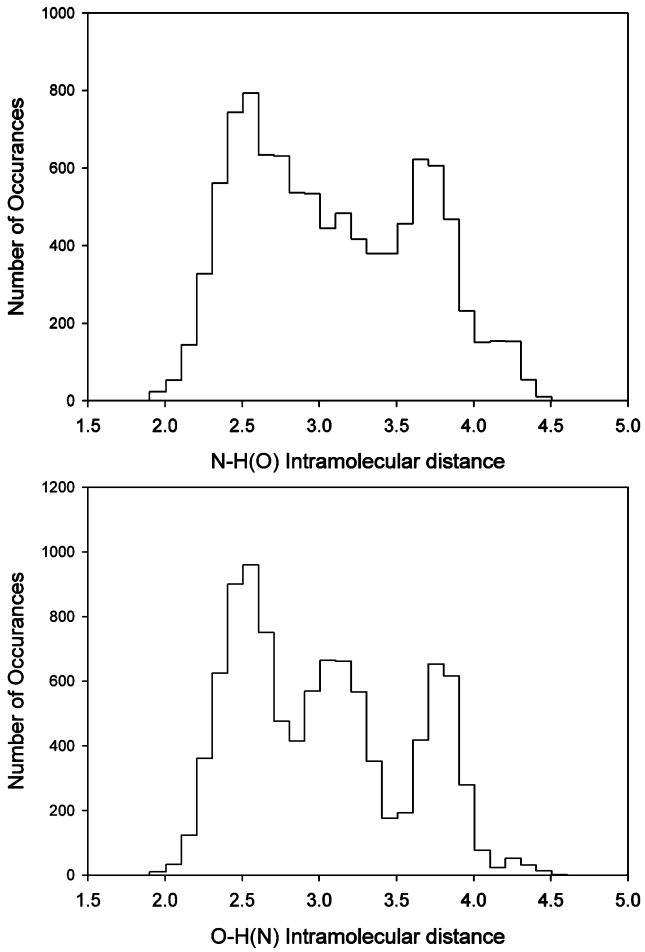

Figure 4. Diagram over intramolecular hydrogen bonds for ethanolamine in infinite dilution aqueous solution at 298 K. The O−H(N) diagram only counts interactions with one of the amine group hydrogen atoms.

Five different ensembles were studied. For pure ethanolamine, the ensemble consisted of 512 molecules. To represent 10 mol % ethanolamine in water, an ensemble consisting of 52 ethanolamine molecules and 460 TIP3P water molecules was selected. To study interactions with CO_2, a similar ensemble with 1 CO_2 molecule, 52 ethanolamine molecules, and 460 water molecules was selected. To represent ethanolamine in infinite dilution, an ensemble of 1 ethanolamine molecule and 511 water molecules was selected. Simulation was also carried out for water with an ensemble consisting of 512 TIP3P water molecules.

The time-step in the simulations was set to 0.002 ps. All ensembles were equilibrated for at least 1 ns. Sampling for the pure ethanolamine system was done over 1 ns, for 10 mol % ethanolamine over 4 ns and for the infinite dilution system over 20 ns.

The assignment of conformers was done by defining any angle between 0 and 120° as g, any angle between 120° and 240° as t, and any angle between 240° and 360° as g′. The enthalpy of vaporization was calculated from the following equation

$$\Delta H_{vap} = E_{pot}(g) - (E_{pot}(l)) + RT \quad (6)$$

where $E_{pot}(g)$ and $E_{pot}(l)$ are the potential energies for the gas and the liquid phase, respectively. Gas-phase simulations for a single ethanolamine molecule were carried out over 1×10^6 time steps. For this periodic, boundary conditions and Ewald

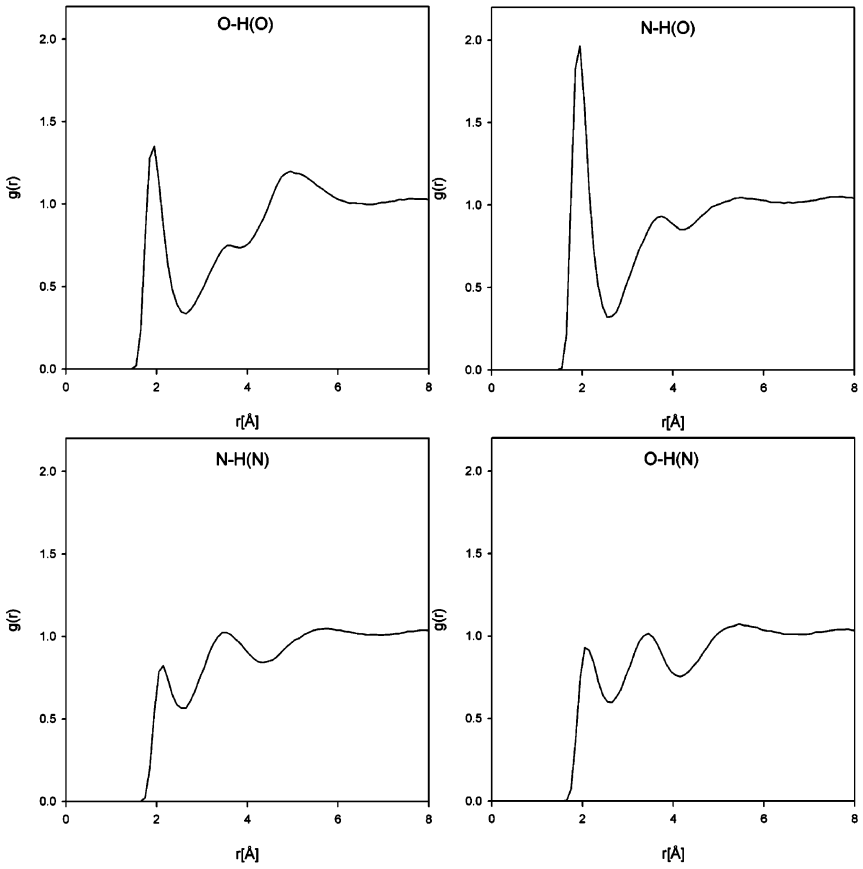

Figure 5. Radial distribution functions for pure ethanolamine at 333 K.

procedure were not applied, and Langevin dynamics were again used to maintain temperature. The output was studied to verify that kinetic energy was evenly distributed over the molecule.

The dielectric constant was calculated from the following equation[22]

$$\epsilon_o = 1 + 3yG_k \tag{7}$$

where

$$y = 4\rho\mu^2/9k_bT \tag{8}$$

and

$$G_k = \frac{\sum_i^N \langle \mu_i \mathbf{M} \rangle}{N\mu^2} \tag{9}$$

here, **M** is the mean dipole moment of the system, μ is the dipole moment, and ρ is the number density. The uncertainty in the dielectric constant has been estimated from a method proposed by Straatsma et al.[23]

The self-diffusion coefficient is calculated from the mean-square displacement of the molecules.

Results

The relative conformer energies in Table 2 and rotational energies in Figure 2 show that the MEAa force field is in good overall agreement with results from quantum mechanical calculations. However, we did not succeed in accurately reproducing all relative conformer energies from quantum mechanical calculations. In Table 3, calculated liquid properties of the MEAa and MEAo force fields together with experimental data are shown.

The MEAa force field has a density that is somewhat higher than the experimental value and a heat of vaporization somewhat lower than the experimental value. We were not able to fit both of these properties accurately with our present fitting procedure. Simulations with varying force field suggest that the heat of vaporization and, to a lesser extent, the density of ethanolamine depend on the conformer distribution and the liquid structure. The failure of the MEAa force field to accurately reproduce these properties may be due to some extent to some subtle failure in reproducing the conformer distribution or bonding. While improved agreement with the experimental data could certainly be achieved by fitting more of the parameters, there is a risk that improved agreement would be achieved for the wrong reasons. We have therefore chosen to keep parameters within the limits suggested by quantum mechanical calculations and general force fields. The dielectric constant of MEAa appears to be in reasonable agreement with the experimental value. For the MEAo force field, it can be seen from Table 3 that the agreement with experimental data is somewhat poor.

Table 3 also shows the densities of water and 10 wt % ethanolamine in aqueous solution at 333 K. In the simulations of 10 wt % ethanolamine, we obtain a density around 2% higher than that for water, while experiments suggests this difference is around 1%. This indicates that the structural effect of ethanolamine on the solvent structure is somewhat overstated.

It can also be seen from Table 3 that the density of water is underestimated in the simulations. One cause of this is discrepancies between the present code and the code in which the TIP3P model was parametrized. A second factor is that the TIP3P model was parametrized at room temperature and overestimates the change in density with temperature.[26]

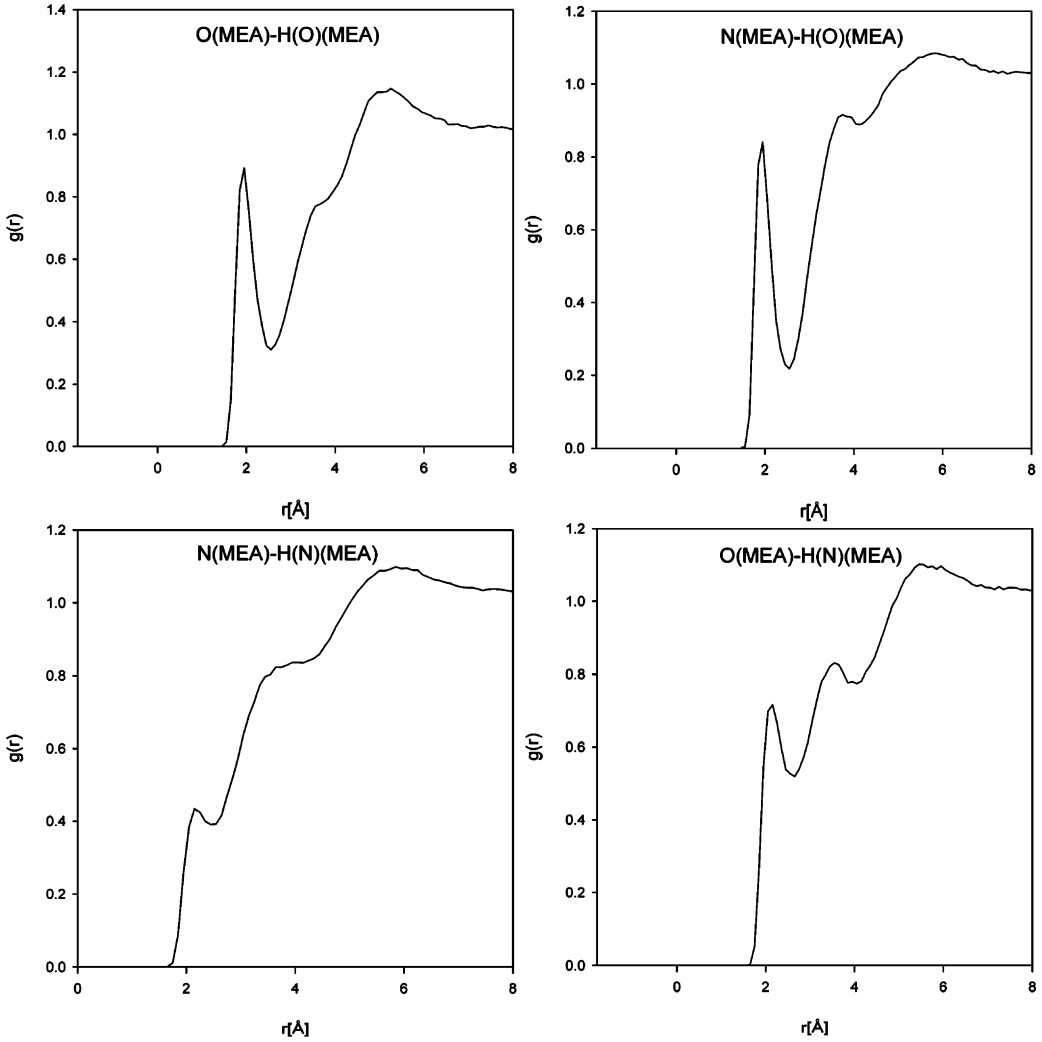

Figure 6. Ethanolamine−ethanolamine radial distribution functions for 10 mol % ethanolamine in water.

Table 4 shows conformer populations for pure ethanolamine and ethanolamine in infinite dilution in water. The pure ethanolamine results are for both MEAa and MEAo at 333 K, while the results for aqueous solution are for MEAa at 298 K. All conformers except tTt have two symmetrical forms. If the conformer space was perfectly sampled, then it would be expected that the symmetrical forms had the same population and the population ratio between the symmetrical forms is an indicator of the quality of the sampling. For pure ethanolamine, the largest ratio in population between symmetrical forms was 1.09; this suggests good overall sampling. For ethanolamine in infinite dilution, the highest ratio was 2.9 (for gTt), suggesting that the sampling for some conformers is limited and that the results are more uncertain.

The results for pure ethanolamine suggest that a number of conformers have significant populations. Conformers with a gauche form of the N−C−C−O dihedral do however dominate with fractions varying between 67% and 87% of the total conformer population. The results suggest that the tGg′ conformer (shown in Figure 1) is the most populated. For ethanolamine in infinite dilution, the results are not that different from those of pure ethanolamine. The proportion of conformers with a gauche form is the same, and tGg′ is again the most populated conformer. In Table 4, conformer populations calculated from the SM 5.42R solvation model[27] and quantum mechanical free energies reported by Vorobyov et al.[18] are also shown. The overall agreement between the simulation and continuum model results is reasonably good. The total population with gauche forms of N−C−C−O dihedral is about the same. In the continuum model results, gGt and tGt are the most populated conformers, while in the simulation results, it is tGg′ and tGg.

In Figure 4, the distribution of intramolecular hydrogen bonds for ethanolamine in infinite dilution are shown. For comparison, it can be noted that in the gas phase the g′Gg′ conformer has a N−H(O) hydrogen bond length of 2.3 Å and the tGt conformer has a O−H(N) bond of 2.64 Å. It can be seen in Figure 4 that there are significant occurrences of bond lengths close to these optimal values. Whereas in the gas phase the g′Gg′ conformer and the N−H(O) hydrogen bond would dominate, the data in Figure 4 show that the O−H(N) hydrogen bond becomes more prevalent in solution. This is consistent with the conformer distribution results.

Radial distribution functions for pure ethanolamine are shown in Figure 5 and Figure 8. In Figure 5, the interactions relevant to hydrogen bond formation are shown. Through comparison of the different radial distributions, it appears that the dominant hydrogen bond in the liquid is of the H(O)−N type. Bonding of the H(O) −O type is also significant. Hydrogen bonds involving the H(N) atoms appear to relatively weak.

In Figures 6, 7, and 8,the radial distribution functions for 10 mol % ethanolamine in water are shown. Figures 6 and 8 show ethanolamine−ethanolamine interactions, while ethanolamine−water interactions are shown in Figure 7. All together, the radial

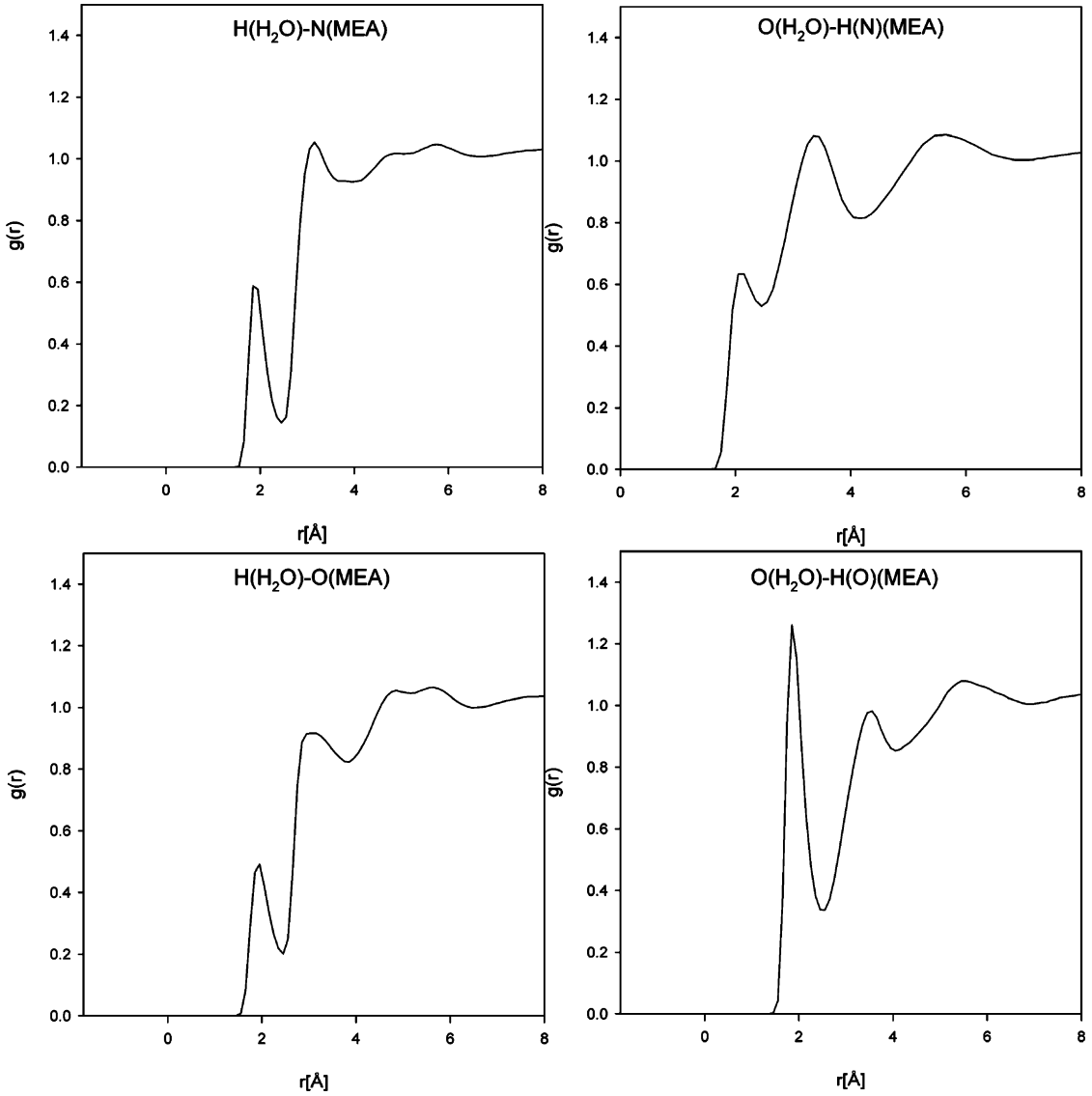

Figure 7. Ethanolamine−water radial distribution functions for 10 mol % ethanolamine in water.

distribution functions suggest that the ethanolamine molecules have a preference to be solvated by water molecules. Hydrogen bonding between ethanolamine molecules is for all interactions less pronounced than those for the pure liquid. N−H(N) interactions become significantly less frequent in aqueous solution. Looking at interactions between ethanolamine molecules and water molecules, it can be seen that H(O) on ethanolamine interaction with O(H_2O) is the strongest feature; the H(N) on ethanolamine interaction with O(H_2O) is much weaker. This observation helps to interpret the conformer populations; the alcohol group hydrogen is preferentially bonded to solvent molecules, resulting in a lower population of conformers with intramolecular H(O) −N hydrogen bonds; intramolecular O−H(N) bonds then become a more dominant feature.

In Figure 8, a methyl group−methyl group radial distribution function for pure ethanolamine and aqueous solution is shown. The other methyl group radial distribution functions (C(N) −C(O) and C(O) −C(O)) display the same features as the one shown in Figure 8. In pure ethanolamine, the methyl group interactions appear to be a relatively weak feature. Comparison between radial distributions in Figures 6 and 8 do however suggest that in aqueous solution the methyl group interactions are the most frequent interactions between ethanolamine mol-

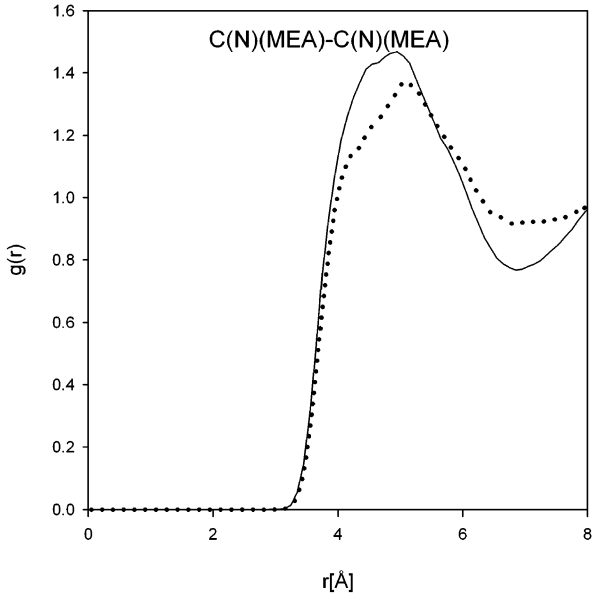

Figure 8. Ethanolamine C(N) −C(N) radial distribution functions. The solid line is for pure liquid, while the dotted line is for 10 mol % aqueous solution.

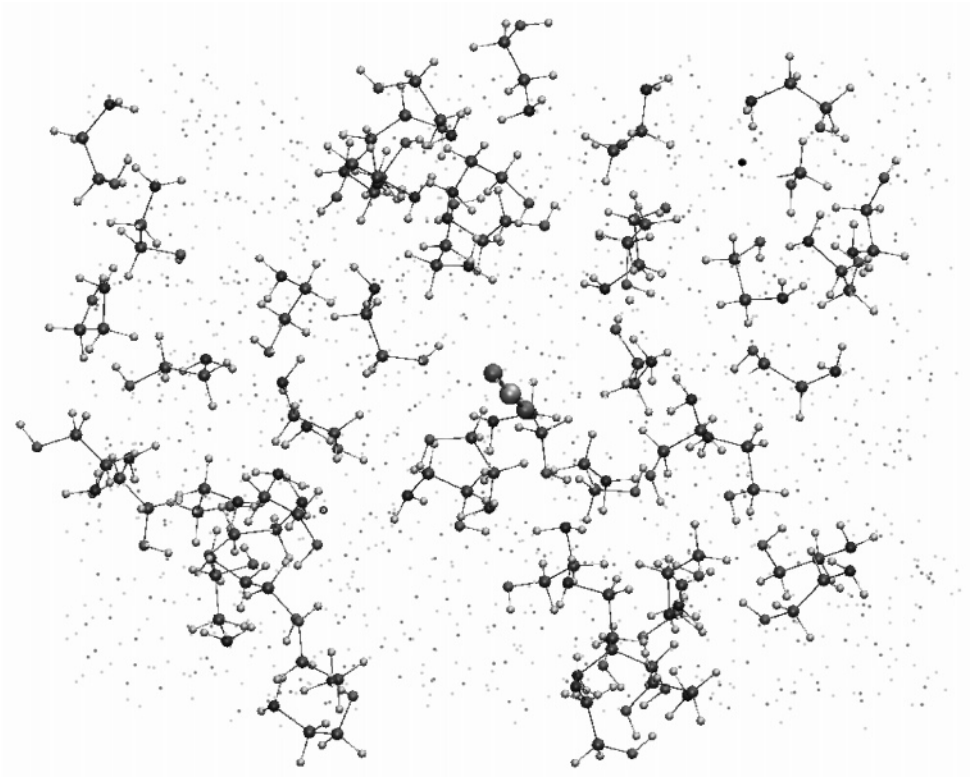

Figure 9. CO_2 (center of figure) in 10 mol % ethanolamine in aqueous solution. Ethanolamine molecules shown in ball and stick representation; water molecules only shown as dark points for O atoms and light points for H atoms.

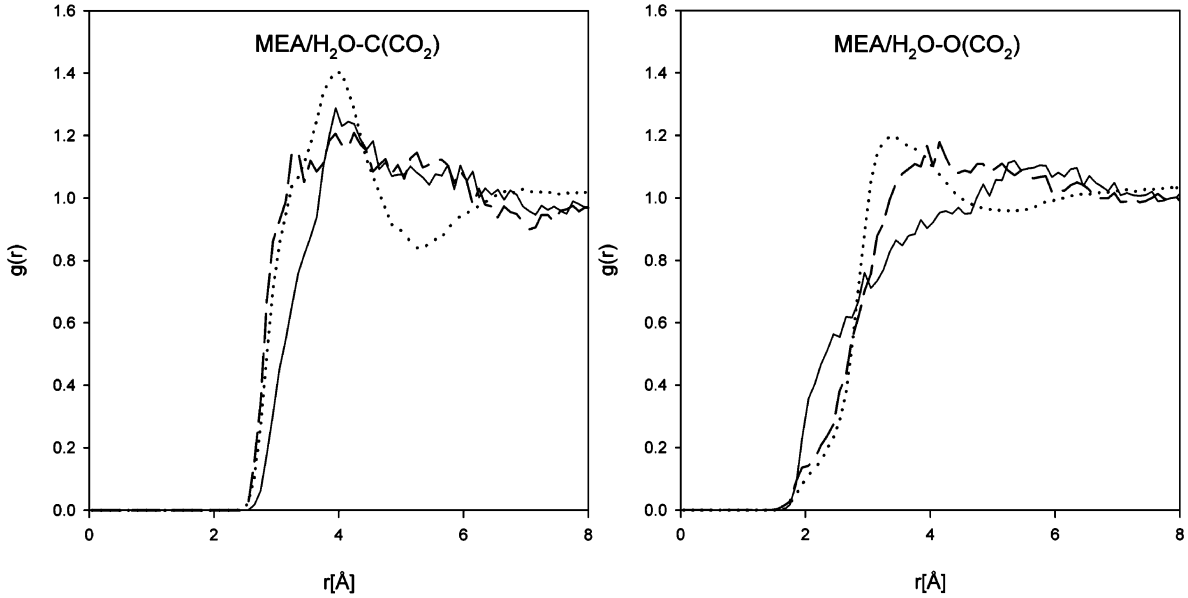

Figure 10. CO_2−ethanolamine−H_2O radial distribution functions at 333 K for 10 mol % ethanolamine in water. Lines in the left plot are as follows: the solid line is $C(CO_2)$ −N(MEA), dashed line is $C(CO_2)$ −O(MEA), and dotted line is $C(CO_2)$−$O(H_2O)$. Lines in the right plot are as follows: the solid line is $O(CO_2)$−H(N)(MEA), dashed line is $O(CO_2)$ −H(O)(MEA), and dotted line is $O(CO_2)$ −$H(H_2O)$.

ecules. This feature is however not so strong as to suggest any significant aggregation of ethanolamine molecules.

It has been suggested that ethanolamine may form dimers in aqueous solution.[29] To assess the extent of ethanolamine dimer formation, the liquid structure of 10 mol % ethanolamine in water at 333 K was analyzed. A search was conducted for pairs of ethanolamine molecules where both the H(O)−N distances were less than 3.3 Å, corresponding to the dimer shown in Figure 3. The presence of such dimers for 10 ethanolamine molecules were checked every 0.2 ps over a 4 ns simulation. Some dimer formation was observed (a snapshot of such a dimer is shown in the Supporting Information); however, the dimers were not stable over time and did not form a significant part of the overall population. The longest observed lifetime for a dimer was 94 ps; the average lifetime was around 20 ps and the overall ratio of ethanolamine molecules in a dimer form was around 0.5%.

The self-diffusion constants of MEAa have been calculated from the simulations. For pure ethanolamine at 333 K, the calculated value is 0.61×10^{-5} cm^2 s^{-1}, while for ethanolamine in infinite dilution at 333 K the calculated value is 4.8×10^{-5} cm^2 s^{-1}. These values do obviously depend on the nature of

the force field, but considering likely biases in the force field, an estimate can be made as to how close these values would be to those for a real system. The TIP3P solvent is known to have a self-diffusion constant that is a factor of around 1.7 higher than the experimental value.[9] For the self-diffusion of ethanolamine in water, the same bias is probably present, scaling the value down by this factor a value of 2.8×10^{-5} cm^2 s^{-1} is obtained. Because the MEAa force field has as previously noted a somewhat high density and a somewhat low heat of vaporization, it is difficult to conclude on whether the force field is overestimating or underestimating the strength of molecular interactions. Given this uncertainty, we suggest an estimate of $(0.6 \pm 0.3) \times 10^{-5}$ cm^2 s^{-1}.

In Figure 9, a snapshot of a CO_2 molecule in 10 mol % ethanolamine in aqueous solution is shown. Radial distribution functions for interactions between CO_2, water, and ethanolamine are shown in Figure 10. The radial distributions suggest that there is no significant difference in the affinity of CO_2 toward ethanolamine and water. It must be kept in mind that CO_2 may bind to ethanolamine according to reaction 1; this possibility is however not captured in the present simulations. If this effect was accounted for, then the radial distribution functions between CO_2 and the amine functionality in the 0−2.5 Å range would most likely be quite different.

From the present results, we can attempt to draw conclusions on the nature of the reaction between CO_2 and ethanolamine. da Silva and Svendsen[12] concluded that the reaction mechanism had no intrinsic barrier. They also suggested that the barrier could arise either from the CO_2 molecule needing to displace the water molecules around the amino group before reacting or from the need for two amine molecules to approach each other sufficiently for a proton transfer to take place. The present results would suggest that, while there is not a significant barrier to the approach of CO_2 to the ethanolamine amino group, this is a somewhat rare event. The low degree of direct interaction between amino functionalities on different molecules would suggest that the likelihood of a base molecule being available for proton transfer is also somewhat low. Taken together this suggests that the kinetics of the reaction is determined by the likelihood that a CO_2 molecule, reacting ethanolamine molecule, and second ethanolamine molecule (base) are sufficiently well aligned that reaction may occur.

Conclusions

Results from the present work suggest that the ethanolamine O−C−C−N dihedral tends to stay predominantly in a gauche conformer both in pure liquid and in aqueous solution. There appears to be a significant degree of intramolecular hydrogen in solution. In aqueous solution, ethanolamine is preferentially solvated by water molecules and there is only limited formation of ethanolamine dimers. Simulations in aqueous solution suggest that CO_2 has a comparable level of affinity to ethanolamine and water. The picture formed of the liquid structure suggests that the kinetics of reaction between CO_2 and ethanolamine may be controlled by the likelihood of three molecules aligning for reaction.

Acknowledgment. This work has been supported by the Norwegian Research Council through post doctoral funding for Eirik F. da Silva.

Supporting Information Available: The force field parameters for CO_2 and a snapshot of the ethanolamine dimer in aqueous solution are given. This material is available free of charge via the Internet at http://pubs.acs.org.

References and Notes

(1) Versteeg, G. F.; Van Dijck, L. A. J.; Van Swaaij, W. P. M. *Chem. Eng. Commun.* **1996**, *144*, 113.

(2) Rao, A. B.; Rubin, E. S. *Environ. Sci. Technol.* **2002**, *36*, 4467.

(3) Button, J. K.; Gubbins, K. E.; Tanaka, H.; Nakanishi, K. *Fluid Phase Equilib.* **1996**, *116*, 320.

(4) Alejandro, J.; Rivera, J. L.; Mora, M. A.; de la Garza, V. *J. Phys. Chem. B* **2000**, *104*, 1332.

(5) da Silva, E. F. *Fluid Phase Equilib.* **2004**, *220*, 239.

(6) Gubskaya, A. V.; Kusilik, P. G. *J. Phys. Chem. A* **2004**, *108*, 7151.

(7) Gubskaya, A. V.; Kusilik, P. G. *J. Phys. Chem. A* **2004**, *108*, 7165.

(8) López-Rendón, R.; Mora, M. A.; Alejandro, J.; Tuckermann, M. E. *J. Phys. Chem. B* **2006**, *110*, 14652.

(9) Guillot, B. *J. Mol. Liq.* **2002**, *101*, 219.

(10) Walser, R.; Mark, A. E.; van Gunsteren, W. F. *J. Chem. Phys.* **2000**, *112*, 10450.

(11) Jorgensen, W. L.; Maxwell, D. S.; Tirado-Rives, J. *J. Am. Chem. Soc.* **1996**, *118*, 11225.

(12) da Silva, E. F.; Svendsen, H. F. *Ind. Eng. Chem. Res.* **2004**, *43*, 3413.

(13) Kirschner, K. N.; Woods, R. J. *Proc. Natl. Acad. Sci. U.S.A.* 98, 10541.

(14) Wang, J.; Wolf, R. M.; Caldwell, J. W.; Kollman, P. A.; Case, D. A. *J. Comput. Chem.* **2004**, *25*, 1157.

(15) Singh, U. C.; Kollman, P. A. *J. Comp. Chem.* **1984**, *5*, 129.

(16) Frisch, M. J.; Trucks, G. W.; Schlegel, H. B.; Scuseria, G. E.; Robb, M. A.; Cheeseman, J. R.; Zakrzewski, V. G.; Montgomery, J. A., Jr.; Stratmann, R. E.; Burant, J. C.; Dapprich, S.; Millam, J. M.; Daniels, A. D.; Kudin, K. N.; Strain, M. C.; Farkas, O.; Tomasi, J.; Barone, V.; Cossi, M.; Cammi, R.; Mennucci, B.; Pomelli, C.; Adamo, C.; Clifford, S.; Ochterski, J.; Petersson, G. A.; Ayala, P. Y.; Cui, Q.; Morokuma, K.; Malick, D. K.; Rabuck, A. D.; Raghavachari, K.; Foresman, J. B.; Cioslowski, J.; Ortiz, J. V.; Baboul, A. G.; Stefanov, B. B.; Liu, G.; Liashenko, A.; Piskorz, P.; Komaromi, I.; Gomperts, R.; Martin, R. L.; Fox, D. J.; Keith, T.; Al-Laham, M. A.; Peng, C. Y.; Nanayakkara, A.; Challacombe, M.; Gill, P. M. W.; Johnson, B.; Chen, W.; Wong, M. W.; Andres, J. L.; Gonzalez, C.; Head-Gordon, M.; Replogle, E. S.; Pople, J. A. *Gaussian 98*, revision A.9; Gaussian, Inc.: Pittsburgh, PA, 1998.

(17) Jorgensen, W. L.; Rizzo, R. C. *J. Am. Chem. Soc.* **1999**, *121*, 4827.

(18) Vorobyov, I.; Yappert, M. C.; DuPre, D. B. *J. Phys. Chem. A* **2002**, *106*, 668.

(19) Jorgensen, W. L.; Chandrasekhar, J.; Madura, J. D.; Impey, Klein, M. L. *J. Chem. Phys.* **1983**, *79*, 926.

(20) Harris, J. G.; Yung, K. H. *J. Phys. Chem.* **1995**, *99*, 12021.

(21) Case, D. A.; Darden, T. A.; Cheatham, T. E., III; Simmerling, C. L.; Wang, J.; Duke, R. E.; Luo, R.; Merz, K. M.; Pearlman, D. A.; Crowley, M.; Walker, R. C.; Zhang, W.; Wang, B.; Hayik, S.; Roitberg, A.; Seabra, G.; Wong, K. F.; Paesani, F.; Wu, X.; Brozell, S.; Tsui, V.; Gohlke, H.; Yang, L.; Tan, C.; Mongan, J.; Hornak, V.; Cui, G.; Beroza, P.; Mathews, D. H.; Schafmeister, C.; Ross, W. S.; Kollman, P. A. *AMBER 9*; University of California: San Francisco, CA, 2006.

(22) Höchtl, P.; Boresch, S.; Bitomsky, W.; Steinhauser, O. *J. Chem. Phys.* **1998**, *109*, 4927.

(23) Straatsma, T. P.; Berendsen, H. J. C.; Stam, A. *J. Mol. Phys.* **1986**, *57*, 89.

(24) Cheng, S.; Meisen, A., Chakma, A. Hydrocarbon Processing, 1996, February, 81.

(25) Austgen, D. M.; Rochelle, G. T.; Peng, X.; Chen, C.-C. *Ind. Eng. Chem. Res.* **1989**, *28*, 1060.

(26) Jorgensen, W. J.; Jenson, C. *J. Comp. Chem.* **1997**, *19*, 1179.

(27) Hawkins, G. D.; Zhu, T.; Li, J.; Chambers, C. C.; Giesen, D. J.; Liotard, D. A.; Cramer, C. J.; Truhlar, D. G. *Universal Solvation Models in Combined Quantum Mechanical and Molecular Mechanical Methods*; Gao, J., Thompson, M. A., Eds.; American Chemical Society: Washington DC, 1998; p 201.

(28) Xidos, J. D.; Li, J.; Zhu, T.; Hawkins, G. D.; Thompson, J. D.; Chuang, Y.-Y.; Fast, P. L.; Liotard, D. A.; Rinaldi, D.; Cramer, C. J.; Truhlar, D. G. *Gamesol*, version 3.1; University of Minnesota: Minneapolis, MN, 2002, based on the General Atomic and Molecular Electronic Structure System (GAMESS) as described in Schmidt, M. W.; Baldridge, K. K.; Boatz, J. A.; Elbert, S. T.; Gordon, M. S.; Jensen, J. H.; Koseki, S.; Matsunaga, N.; Nguyen, K. A.; Su, S. J.; Windus, T. L.; Dupuis, M.; Montgomery, J. A. *J. Comp. Chem.* **1993**, *14*, 1347.

(29) Mate-Divo, M.; Barcza, L. *Z. Phys. Chem.* **1995**, *190*, 223.